ARL

...ubic Aerodynamics CFD Analysis for 120-mm Hypersonic KE Projectile Design

Bernard J. Guidos

...LCAST-94

September 1994

NOTICES

Destroy this report when it is no longer needed. DO NOT return it to the originator.

Additional copies of this report may be obtained from the National Technical Information Service, U.S. Department of Commerce, 5285 Port Royal Road, Springfield, VA 22161.

The findings of this report are not to be construed as an official Department of the Army position, unless so designated by other authorized documents.

The use of trade names or manufacturers' names in this report does not constitute indorsement of any commercial product.

REPORT DOCUMENTATION PAGE

Form Approved
OMB No. 0704-0188

1. AGENCY USE ONLY *(Leave blank)*	2. REPORT DATE	3. REPORT TYPE AND DATES COVERED
	September 1994	Final, September 1992 - April 1994

4. TITLE AND SUBTITLE
Static Aerodynamics CFD Analysis for 120-mm Hypersonic KE Projectile Design

5. FUNDING NUMBERS
PR: 1L162618AH80

6. AUTHOR(S)
Bernard J. Guidos

7. PERFORMING ORGANIZATION NAME(S) AND ADDRESS(ES)
US Army Research Laboratory
ATTN: AMSRL-WT-PB
Aberdeen Proving Ground, MD 21005-5066

8. PERFORMING ORGANIZATION REPORT NUMBER

9. SPONSORING/MONITORING AGENCY NAMES(S) AND ADDRESS(ES)
US Army Research Laboratory
ATTN: AMSRL-OP-AP-L
Aberdeen Proving Ground, MD 21005-5066

10.SPONSORING/MONITORING AGENCY REPORT NUMBER
ARL-MR-184

11. SUPPLEMENTARY NOTES

12a. DISTRIBUTION/AVAILABILITY STATEMENT
Approved for public release; distribution is unlimited.

12b. DISTRIBUTION CODE

13. ABSTRACT *(Maximum 200 words)*

Computational fluid dynamics (CFD) predictions of static aerodynamic coeffients for large caliber (120-mm) M829-like cone-cylinder-flare kinetic energy (KE) projectile shapes are presented. Zero-yaw drag and static pitch-plane aerodynamic coefficients are presented for velocities in the range 1.5 to 3.0 km/sec for several flare angles. The aerodynamic coefficients are required to assess the velocity retardation and static stability of candidate configurations that use the M829 projectile as a basis for design. Comparisons of the aerodynamic coefficients are made with those of the fielded M829 projectile, and a preliminary evaluation is made of the performance of these shapes in hypersonic flight.

14. SUBJECT TERMS	15. NUMBER OF PAGES
Computational fluid dynamics, supersonic flow, kinetic energy projectiles, aerodynamics	38
	16. PRICE CODE

17. SECURITY CLASSIFICATION OF REPORT	18. SECURITY CLASSIFICATION OF THIS PAGE	19. SECURITY CLASSIFICATION OF ABSTRACT	20. LIMITATION OF ABSTRACT
UNCLASSIFIED	UNCLASSIFIED	UNCLASSIFIED	UL

INTENTIONALLY LEFT BLANK.

TABLE OF CONTENTS

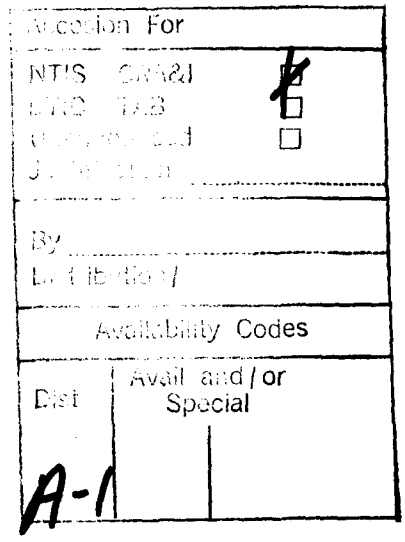

INTENTIONALLY LEFT BLANK.

LIST OF FIGURES

INTENTIONALLY LEFT BLANK.

1. INTRODUCTION

Hypersonic launch and flight technology for large caliber weapons systems, both conventional and nonconventional, continues to be developed within the U.S. Army research community. The hypersonic flight regime and the accompanying violent launch environment pose formidable challenges for projectile designers. The current families of kinetic energy (KE) projectiles were designed for supersonic, rather than hypersonic, applications. One major problem with the current finned KE rounds is that the fins are expected to fail because of excessive heating and structural loading in the hypersonic launch regime. Finned afterbody modification appears to be inevitable, and the relative merits of finned versus flared afterbodies require close examination.

The M829 projectile is one of several large caliber long-rod finned KE rounds being considered as a starting point in the design of the new generation of hypersonic projectiles. The M829, while not the most lethal (or longest) KE projectile in the 120-mm family, provides a good starting point for hypersonic projectile design. The M829 is less costly than the more lethal KE rounds and plays a major role for engagement against a variety of heavy armor targets. In addition, rod bending and buckling are of less concern for the M829 compared to the longer rounds – characteristics that may be valuable in the hypersonic launch regime.

In this report, possible geometry modifications for the M829 finned afterbody are examined in order to generate a set of guidelines for aerodynamic performance. Simple flared afterbody configurations are attractive because of their potential to reduce the heating and structural concerns associated with fins. Flared bodies provide less stability than finned afterbodies (for equivalent drag), but flared afterbodies may still achieve the required terminal effect if the launch velocity is substantially higher than that of the current launch systems.

The objective of this report is to present computed zero-yaw drag and small-yaw static pitch-plane aerodynamic coefficients of a conceptual modified M829 projectile, in which the fins have been replaced by a flare. The aerodynamic coefficients are computed using an in-house Parabolized Navier-Stokes (PNS) computational technique, which is briefly outlined. Results are presented for velocities in the range 1.5 to 3.0 km/sec, for flare angles as great as 20°. Base drag estimates are added to the PNS results to form total drag coefficients. The coefficients are compared to M829 computational results and range firings, and observations are made of the drag-stability trade-off between the configurations.

2. CONFIGURATIONS AND FLIGHT CONDITIONS

Two configurations are examined. The first is the M829 projectile, which is a fielded, fin-stabilized, long-rod KE projectile fired from a 120-mm gun tube. The second is an M829-like cone-cylinder-flare configuration (identified here as F829), which is a conceptual hypervelocity projectile design. The computational model of the M829 projectile (see Figure 1) is a simplified version of the actual model. The F829 model (see Figure 2) is identical to the M829 model except that the fins are replaced by a flare.

Both models possess an 8° conical nose section, followed by a cylindrical section of diameter 27.05 mm (1 caliber). The total model length is about 23 calibers. The actual blunt nosetip is replaced by an extended, pointed, conical nosetip. In the current study, all models are assumed to possess the same center of gravity (CG), 12.76 calibers from the pointed nosetip.

The M829 model has six uncanted fins with a sweep angle of approximately 71° (i.e., a fin angle of 19°) equally distributed around the body and aligned with the projectile axis. The sabot grooves on the cylindrical portion of the actual configuration are replaced with a smooth surface. No leading edge or trailing edge bevels are included in the computational model. The overhanging fin of the actual projectile is modeled with the cylinder extending to the fin trailing edge, as shown in Figure 1. The resulting fin gap is modeled as a solid structure.

The flare angle of the F829 model is varied from 0° to 20°. It is assumed that the flow does not separate at the cylinder-flare juncture. A small fillet is added to the computational geometry at the cylinder-flare juncture to impose a smooth, attached flow. The computed flow field must remain attached as a numerical stability requirement of the PNS technique. From a projectile design standpoint, massive flow separation ahead of the flare is probably not desirable, since it can induce loss of lift and local areas of large aerodynamic heating.

Computational results for the F829 configuration are presented for freestream velocities 1.5, 2.0, and 3.0 km/sec. Computational results for the M829 configuration are shown for freestream velocities 1.5, 1.7, and 2.0 km/sec. The service launch velocity of the M829 is approximately 1.7 km/sec, as given in Department of the Army Firing Table FT 120-D-1. The M829 decelerates to a velocity of 1.5 km/sec at a range of approximately 3.0 km.

Atmospheric, sea-level, freestream conditions are assumed for all computations. The angle of attack is fixed at either 0° or 2°. The spin rate is fixed at 0 rpm, and the flow is assumed fully turbulent. The wall temperature is specified as 294 K. The Reynolds numbers for the velocities of interest are shown in Table 1.

Table 1. Flight Conditions of Interest

Velocity (km/sec)	Mach No.	Reynolds No. (Re_m)
1.5	4.4	99.6×10^6
1.7	4.9	113.0×10^6
2.0	5.9	133.9×10^6
3.0	8.8	199.6×10^6

3. PARABOLIZED NAVIER-STOKES CFD TECHNIQUE

3.1 Overview. The PNS technique has been adapted and extensively used within the U.S. Army Research Laboratory (ARL) (formerly the Ballistic Research Laboratory) and is a powerful computational fluid dynamics (CFD) research tool for predicting supersonic and hypersonic projectile aerodynamics. The PNS technique is a space-marching (as opposed to a time-marching) technique; that is, one numerical integration sweep is made from the nosetip of the projectile to the base to obtain a single steady state solution. A typical solution for a three-dimensional geometry at angle of attack in this study was generated using about 1 or 2 hours of processing time on the Cray X-MP computer. Axisymmetric configurations at 0° angle of attack took less than 10 minutes each.

The PNS technology was first applied to U.S. Army projectiles to compute static pitch-plane and Magnus coefficients for spinning and non-spinning shell and for wind tunnel models at various angles of attack (Sturek & Schiff 1981; Schiff & Sturek 1981). Similar applications were made to shell at moderate angle of attack and to finned KE projectiles (Weinacht, Guidos, et al., 1985, 1986). The technique was modified to compute roll characteristics of finned KE projectiles with exact fin geometry using a rotating coordinate frame (Weinacht & Sturek 1988). Further modifications were added to compute the pitch damping of axisymmetric (Weinacht, Sturek, & Schiff 1991) and finned (Weinacht & Sturek 1990) projectiles, including the M829 configuration, using a coning coordinate frame.

The PNS approach has also been used for other in-house research and design studies. Blunt nosetip solutions were marched downstream using the PNS code and were compared to wind tunnel data (Guidos, Weinacht, & Dolling 1990). Studies have also been made for electro-magnetic launch projectiles (Weinacht 1989), small caliber training rounds (Guidos 1987), and solid fuel ramjet external flow (Guidos 1989). More recently, efforts have focused on perfect gas, hypersonic heat transfer for large caliber finned KE projectiles and cone-cylinder-flares (Guidos & Weinacht 1993).

3.2 Computational Approach. The PNS technique introduced by Schiff and Steger (1979) is a three-dimensional, finite difference, viscous flow solution procedure for attached supersonic and hypersonic flow fields. The PNS technique spatially integrates the dimensionless, transformed, steady, thin-layer, mass-averaged Navier-Stokes equations in strong conservation law form. The governing equations represent steady state conservation of mass, momentum, and energy in transformed coordinates for large Reynolds number flows. The Cartesian form of the equations is

$$\frac{\partial \hat{E}_s}{\partial \xi} + \frac{\partial \hat{F}}{\partial \eta} + \frac{\partial \hat{G}}{\partial \zeta} = \hat{R}e^{-1}\frac{\partial \hat{S}}{\partial \zeta} \tag{1}$$

These equations were recast in cylindrical coordinates and applied by Rai and Chaussee (1983). The major advantage is that the cylindrical coordinate formulation requires only three circumferential grid planes for axisymmetric flow cases within the framework of the bilateral symmetry that is imposed. The cylindrical form of the governing equations is

$$\frac{\partial \hat{E}_s}{\partial \xi} + \frac{\partial \hat{F}}{\partial \eta} + \frac{\partial \hat{G}}{\partial \zeta} + \hat{H}_c = \hat{R}e^{-1}\left(\frac{\partial \hat{S}}{\partial \zeta} + \hat{S}_c\right) \tag{2}$$

The vectors $\hat{E}_s$, $\hat{F}$, and $\hat{G}$ contain the transformed inviscid fluxes. $\hat{E}_s$ is a modified flux vector resulting from the subsonic sublayer approximation (Schiff & Steger 1979). The vector $\hat{S}$ is the transformed vector of viscous terms that results from the thin layer approximation. The vectors $\hat{H}_c$ and $\hat{S}_c$ contain inviscid and viscous source terms, respectively, resulting from the cylindrical coordinate formulation. The components of the vectors for the Cartesian formulation are given in many sources, including Schiff & Steger. The components of all the vectors for the cylindrical formulation are given by Weinacht and Sturek (1990). The three transformed coordinates are: $\xi = \xi(x)$, the axial (marching); $\eta = \eta(x, y, z)$, the circumferential coordinate; and $\zeta = \zeta(x, y, z)$, the radial coordinate. The transposed vector of dependent variables is defined as

$$\bar{Q} = [\rho, \rho u, \rho v, \rho w, \varepsilon] \tag{3}$$

in which the density is ρ; the axial, circumferential, and radial velocity components are are u, v, and w, respectively; and the total energy per unit volume is ε.

The solution is obtained at each grid point using the approximately factored, implicit, delta form, finite difference algorithm of Beam and Warming (1978). Second-order central differencing is used in the circumferential and radial directions, and first-order one-sided differencing is used in the marching direction. The solution is advanced downstream by numerically integrating in the main flow direction. Each marching step requires a series

of block tridiagonal matrix inversions (sweeps) in the circumferential and radial directions. Fourth-order explicit smoothing terms are added to suppress high frequency oscillations. Second-order implicit smoothing terms are added to maintain numerical stability in regions of large pressure gradients (such as fin leading edges). Initial conditions for marching are generated using the PNS method in step-back mode (Sturek & Schiff 1981), which assumes conical flow conditions near the nosetip and iteratively refines the solution to satisfy this assumption.

Perfect gas behavior is assumed. Turbulence is accounted for using the two-layer, algebraic eddy viscosity model of Baldwin and Lomax (1978). In that model, the inner wall layer eddy viscosity is computed using a conventional Prandtl mixing length with Van Driest damping. The outer, or wake, layer eddy viscosity is based upon an evaluation of the maximum moment of vorticity and its distance from the wall. The calculation of the eddy viscosity is lagged by one marching step.

The outer boundary, which consists of the bow shock, is shock fitted using the implicit procedure reported by Rai and Chaussee (1983). The capability also exists to capture the bow shock by employing freestream conditions at the outer boundary grid points. The body surface boundary conditions are applied assuming that the spinning and coning rates are zero. The no-slip condition is enforced and the pressure is held constant across the subsonic portion of the boundary layer (i.e., the subsonic sublayer approximation). The energy is defined from the pressure using the perfect gas law. The wall temperature is specified, and the density is determined from the temperature and pressure.

4. RESULTS

Figures 3 through 5 show the computed zero-yaw surface pressures for the F829 configuration with various flare angles, for velocities 1.5, 2.0, and 3.0 km/sec. All the computed pressures reach a maximum value 1 or 2 calibers downstream from forebody-afterbody juncture, then decrease slightly over the remainder of the afterbodies. Figure 6 shows the computed zero-yaw forebody and fin leading edge surface pressures for the M829 projectile for velocities 1.5, 1.7, and 2.0 km/sec. At 1.5 km/sec, a flare angle of 16° is computed to have about the same peak pressure as the M829 fin. At 2.0 km/sec, a flare angle of 20° is computed to have about the same peak pressure as the M829 fin.

The computed pressures and shear stresses are integrated over the entire projectile surface to form a set of aerodynamic force and moment coefficients at 0° and 2° angle of attack. These forces and moments do not include contributions and effects attributable to the blunt

nosetip, sabot grooves, leading and trailing edge bevels, base, or (in the case of the finned projectile) fin trailing edge. The drag force yielded by PNS is referred to as the "forebody" drag coefficient, $C_{D_{o_f}}$.

The base drag is estimated using an average base pressure correlation from McCoy (1981), with the base diameter specified to be 1 caliber regardless of the actual flare angle. For the finned geometry, the presence of fins is ignored. It is noted that finned and flared geometries have lower base pressure than a cylindrical base with no fins (Heyser, Maurer, & Oberdorffer, 1966; Sedney, 1966). The estimated base pressure is then integrated over the actual base area (and fin trailing edges, if applicable) of the individual configurations. The estimated base pressure values obtained from this approach are given in Table 2. The resulting base drag coefficient, $C_{D_{o_B}}$, is then added to the forebody drag coefficient to obtain the total zero-yaw drag coefficient, C_{D_o}. The values of these and all the computed aerodynamics coefficients are shown in Tables 3 and 4.

Table 2. Estimated Base Pressures

Velocity (km/sec)	Base Pressure p_B/p_∞
1.5	.146
1.7	.118
2.0	.080
3.0	.035

Table 3. Computed Results - M829 Configuration

V (km/sec)	$C_{D_{of}}$	$C_{D_{oB}}$	C_{D_o}	C_{N_α}	CP	C_{m_α}
1.5	0.392	0.117	0.509	15.83	17.59	-76.50
1.7	0.389	0.097	0.486	14.64	17.19	-64.85
2.0	0.381	0.070	0.451	12.93	16.50	-48.41

In Figures 7 through 9, the computed F829 zero-yaw forebody drag and viscous (skin friction) and inviscid (pressure) components are shown as a function of flare angle, for velocities 1.5, 2.0, and 3.0 km/sec. For flare angles less than 8°, the viscous component provides more of a drag contribution than the pressure component. For this length of flare, flare angles greater than 8° cause a dramatic increase in the pressure component of forebody drag, resulting in a significant increase in total forebody drag. The forebody drag associated with flare angles greater than 12° is quite large and is probably beyond consideration for KE projectile design purposes. No further results are presented for flare angles greater than 12°.

Table 4. Computed Results - F829 Configuration

V=1.5 km/sec						
Flare Angle	$C_{D_{o_f}}$	$C_{D_{o_B}}$	C_{D_o}	C_{N_α}	CP	C_{m_α}
0°	0.197	0.063	0.260	3.51	4.19	30.09
4°	0.250	0.160	0.410	5.39	10.17	13.96
6°	0.330	0.225	0.555	6.85	12.56	1.37
8°	0.471	0.303	0.774	8.67	14.45	-14.65
10°	0.700	0.392	1.092	10.86	15.90	-34.10
12°	1.050	0.495	1.545	13.41	17.02	-57.06
16°	2.267	0.742	3.009	N/A	N/A	N/A
20°	4.509	1.052	5.561	N/A	N/A	N/A

V=2.0 km/sec						
Flare Angle	$C_{D_{o_f}}$	$C_{D_{o_B}}$	C_{D_o}	C_{N_α}	CP	C_{m_α}
0°	0.169	0.038	0.207	3.87	5.10	29.64
4°	0.214	0.096	0.310	5.77	10.44	13.39
6°	0.275	0.135	0.410	7.35	12.80	-0.29
8°	0.394	0.181	0.590	9.35	14.65	-17.67
10°	0.591	0.235	0.826	11.73	16.05	-38.60
12°	0.949	0.296	1.245	14.41	17.09	-62.40
16°	2.111	0.444	2.555	N/A	N/A	N/A
20°	4.269	0.630	4.899	N/A	N/A	N/A

V=3.0 km/sec						
Flare Angle	$C_{D_{o_f}}$	$C_{D_{o_B}}$	C_{D_o}	C_{N_α}	CP	C_{m_α}
0°	0.135	0.018	0.153	4.02	5.91	27.55
4°	0.167	0.045	0.212	5.92	10.89	11.09
6°	0.223	0.064	0.287	7.75	13.36	-4.65
8°	0.332	0.086	0.418	10.12	15.23	-25.00
10°	0.528	0.111	0.639	12.82	16.52	-48.20
12°	0.832	0.140	0.972	15.62	17.39	-72.26
16°	1.920	0.210	2.130	N/A	N/A	N/A
20°	3.925	0.297	4.222	N/A	N/A	N/A

In Figure 10, the computed F829 zero-yaw drag coefficients are plotted as a function of Mach number, with flare angle as a parameter. Comparison is made with the computed and measured drag coefficients for the M829 projectile. The measured data are obtained from standard yaw-drag fits of unpublished M829 range firings performed by F.J. Brandon at Aberdeen Proving Ground in 1983, using the equations of free flight motion (Murphy 1963). The comparison between computation and experiment is within 10-15%. At the current launch velocity, the drag coefficient of the F829 with a 6° flare is shown to be comparable to the drag coefficient of the M829. At that same velocity, the drag coefficient of the F829 with a 10° flare is about twice as large as the drag coefficient of the M829.

Figures 11 through 13 show the computed F829 and M829 normal force coefficient (C_{N_α}), center of pressure (CP), and pitching moment coefficient (C_{m_α}), respectively, as functions of Mach number, with flare angle as a parameter. As already noted, the CG of each configuration is assumed to be the same. The measured M829 results are included in each of the three figures. The M829 computed results for C_{N_α} and CP agree to within the scatter of the measured results. The M829 computed results for C_{m_α} show slightly more stability than the measured results, likely attributable to the additional fin and cylinder surface area present in the computational model (discussed in Section 2). The precise values of all the computed pitch-plane coefficients are included in Tables 3 and 4.

Figures 11 through 13 also show that the F829 configurations with flare angles less than 6° are statically unstable at all the velocities considered here. It is true that a flare angle of 12° does give the F829 configuration a CP value comparable to the M829 near the current launch velocity, but with more than twice the drag. On the other hand, an F829 flare angle small enough to yield drag comparable to the M829 is probably statically unstable.

The finned (M829) and the flared (F829) configurations show different trends with respect to velocity. For the M829 configuration, CP decreases with increasing velocity; for the F829 configurations, CP increases (although the increase is quite small). Strictly speaking, as the velocity increases into the hypersonic regime, a smaller flare angle is required to provide the F829 with CP values comparable to the M829. However, it has yet to be determined whether the static stability of the M829 is sufficient at these higher velocities.

If the current launch level of CP for the M829 must be maintained for higher-than-current launch velocities, then necessary design considerations would impact the afterbody design, regardless of fins or flares. For a finned afterbody, fin planform area (i.e., lift) would need to be increased or the current fins would somehow need to be moved rearward. For a flared afterbody, a flare angle of 10° or 12° might be required. If terminal velocity is a predominant design consideration, then the velocity retardation of the designs with equivalent CP would

need to be compared to determine muzzle velocity requirements. At the current launch velocities, at least, comparisons clearly show the current M829 fin design to outperform F829 flare configurations in terms of both drag and static stability.

One obvious conclusion that should not be overlooked is that the in-flight variations of static stability of the finned and flared configurations are distinctly different, since the velocity is decreasing. The finned configuration gains static stability during flight, while the flared configuration loses static stability.

Figures 14 through 16 are constructed using these same results, but arranged to show the drag-stability tradeoff for the F829 configuration. These three figures show C_{N_α}, CP, and C_{m_α}, respectively, versus C_{D_o}. Velocity and flare angle are used as parameters. For flare angles above 6°, rearward movement of the CP is accomplished only at the expense of large increases in drag. A rearward shift in CG location for afterbodies with larger flare angles (which would presumably outweigh those with smaller flare angles) would amplify this behavior further for C_{m_α}.

5. CONCLUSION

Parabolized Navier-Stokes results have been presented of zero-yaw drag and small angle of attack static pitch-plane aerodynamics for a M829-like cone-cylinder-flare geometry. The cone-cylinder-flare configuration, designated F829, is a hypothetical configuration in which the fins of an M829 projectile have been replaced by a flare of various angles. Aerodynamics results for the F829 were presented for velocities 1.5, 2.0, and 3.0 km/sec. Additional computational results were presented for the M829 projectile at velocities 1.5, 1.7, and 2.0 km/sec, including aerodynamics range data.

The results show that the aerodynamic design of an M829-like hypersonic projectile configuration may be driven by consideration of the drag-stability trade-off. The use of a flared rather than finned afterbody for an M829-like configuration would require a substantial drag penalty to be paid for the same static stability as the current M829. The total drag of the F829 cone-cylinder-flare configuration with a 6° flare is comparable to that of the M829 projectile, but is barely statically stable, assuming the same CG for both configurations. On the other hand, the F829 with a 12° flare has static stability comparable to the M829 near the current launch velocities, but with more than double the total drag.

As the velocity is increased, a smaller flare angle is required to provide the F829 configuration with static stability comparable to the M829. However, it has yet to be determined that the static stability of the M829 will even be sufficient at higher-than-current veloci-

ties. If the current M829 launch value of CP must be maintained for applications above 2 km/sec, then necessary design changes would impact the afterbody design, regardless of fins or flares. In either case, a reduction in static stability could lead to increased sensitivity to aerodynamic jump or to degradation in penetration because of increased terminal yaw.

For launch velocities at or slightly above the current ordnance velocity, the aerodynamic performance of the F829 flared configurations is significantly below that of the current finned M829. The possibility exists that a flared projectile with less static stability and higher drag than the M829 projectile could still achieve the required terminal effect at significantly higher launch velocities. The results presented here suggest that aerodynamics considerations alone will not provide sufficient impetus to abandon fins in favor of flares in the near future. However, it is generally accepted that the continued use of fins for hypersonic applications will require improved aerothermal and/or structural integrity.

The precise in-flight behavior of candidate designs will depend upon additional factors not specifically addressed here, such as the exact physical properties and dynamic aerodynamics coefficients such as pitch damping. The aerodynamics coefficients for the configurations presented here provide a valuable starting point for designers to assess velocity retardation and static stability for anticipated hypersonic launch velocities.

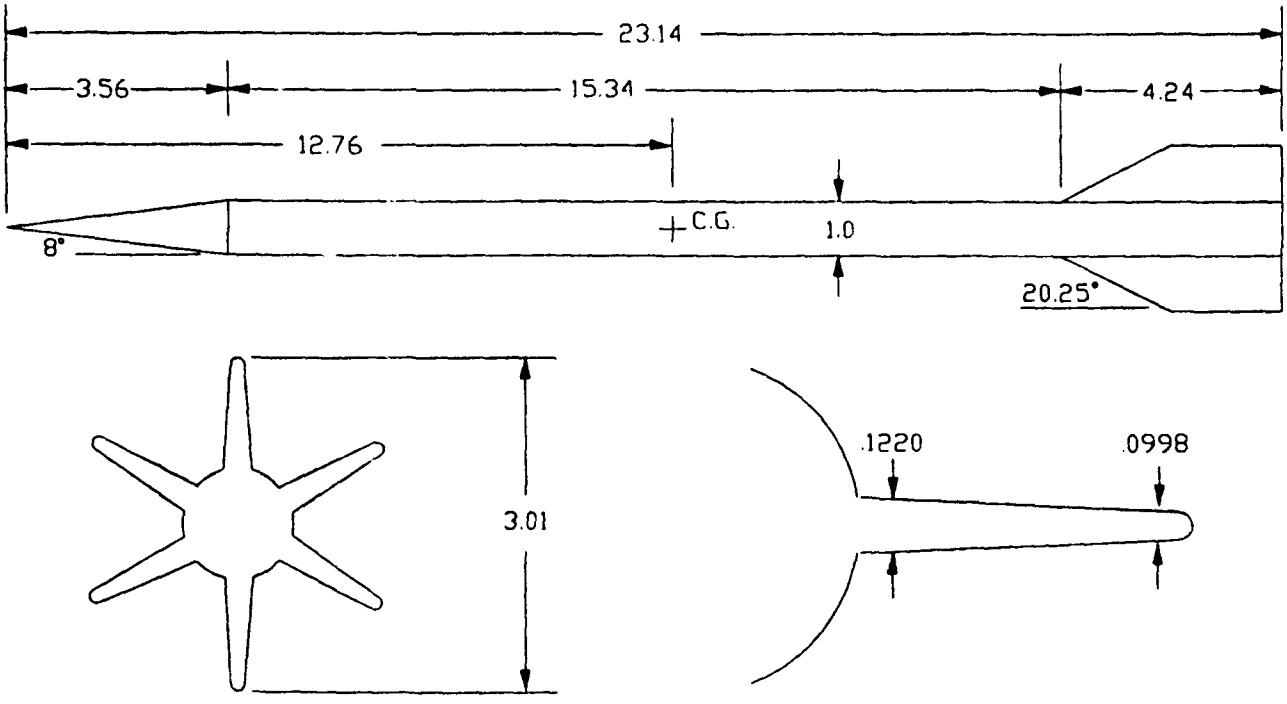

Figure 1. Schematic of M829 Projectile Configuration

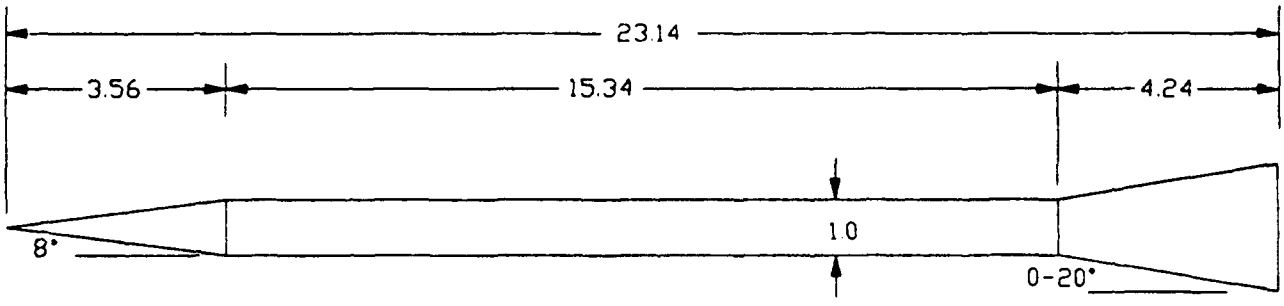

All Dimensions in Calibers (One Caliber=27.05mm)

Figure 2. Schematic of F829 Cone-Cylinder-Flare Configuration

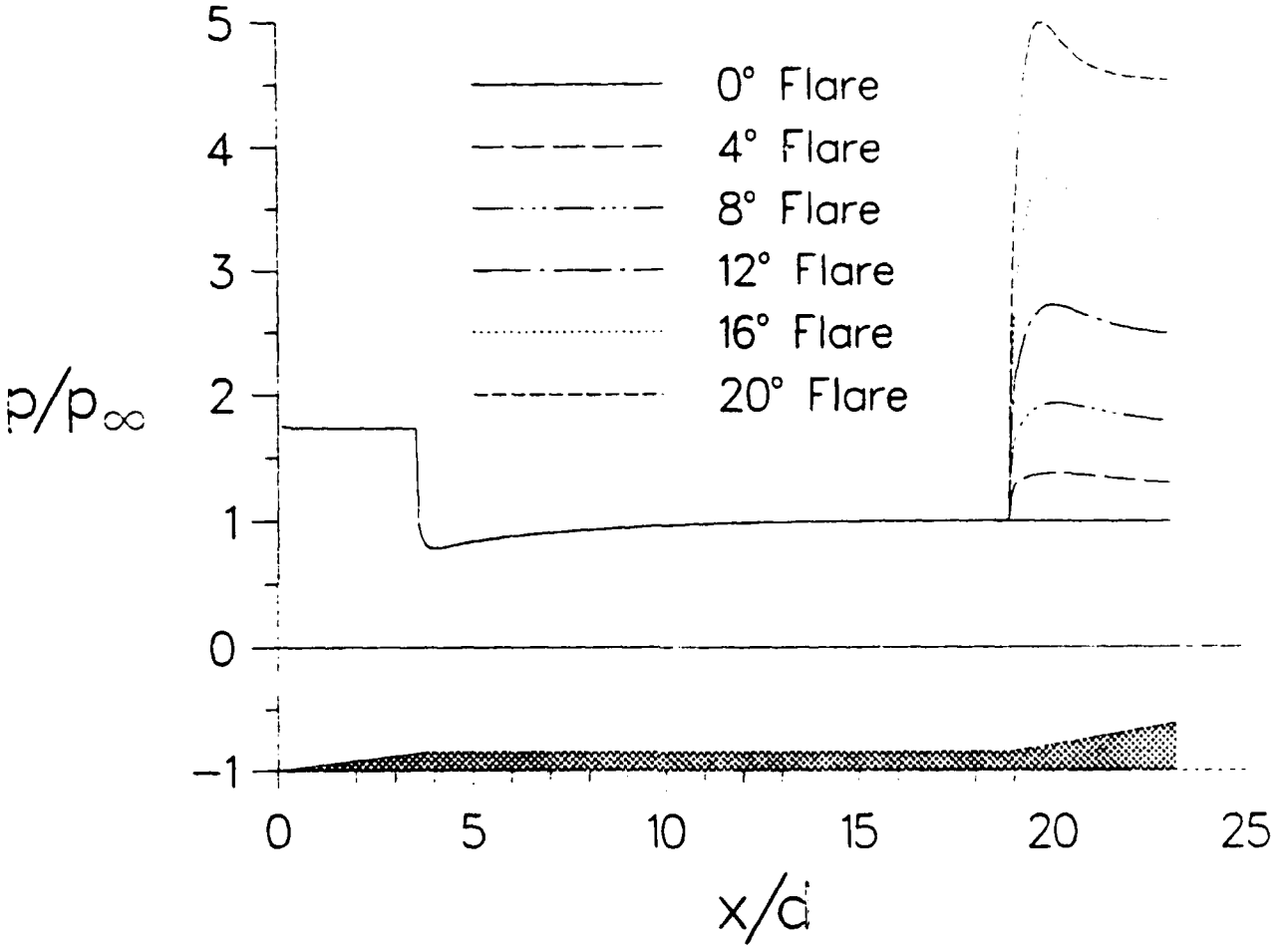

Figure 3. Computed Surface Pressure for F829 With Various Flare Angles, V_∞=1.5 km/sec, $\alpha = 0°$

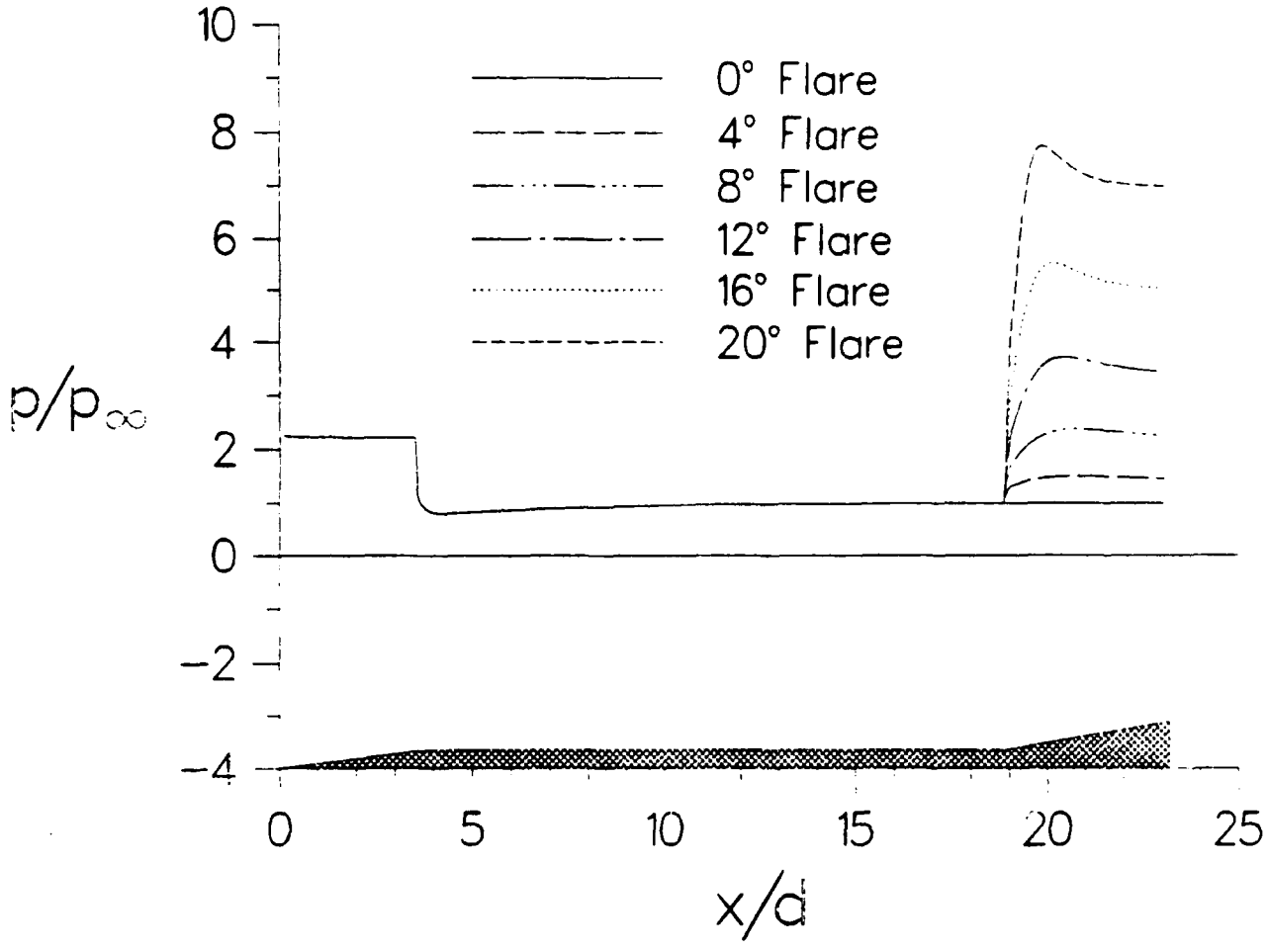

Figure 4. Computed Surface Pressure for F829 With Various Flare Angles, V_∞=2.0 km/sec, $\alpha = 0°$

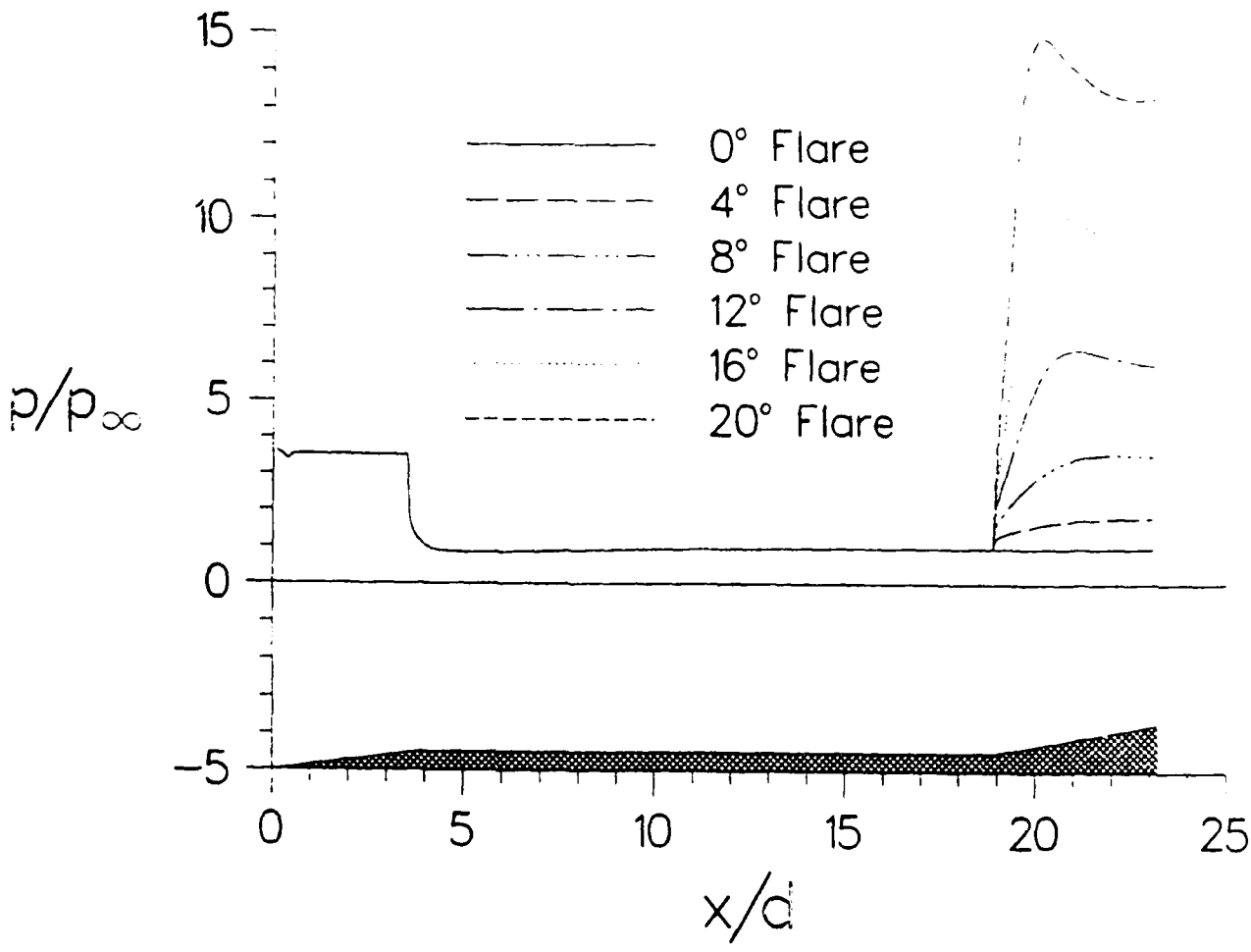

Figure 5. Computed Surface Pressure for F829 With Various Flare Angles, V_∞=3.0 km/sec, $\alpha = 0°$

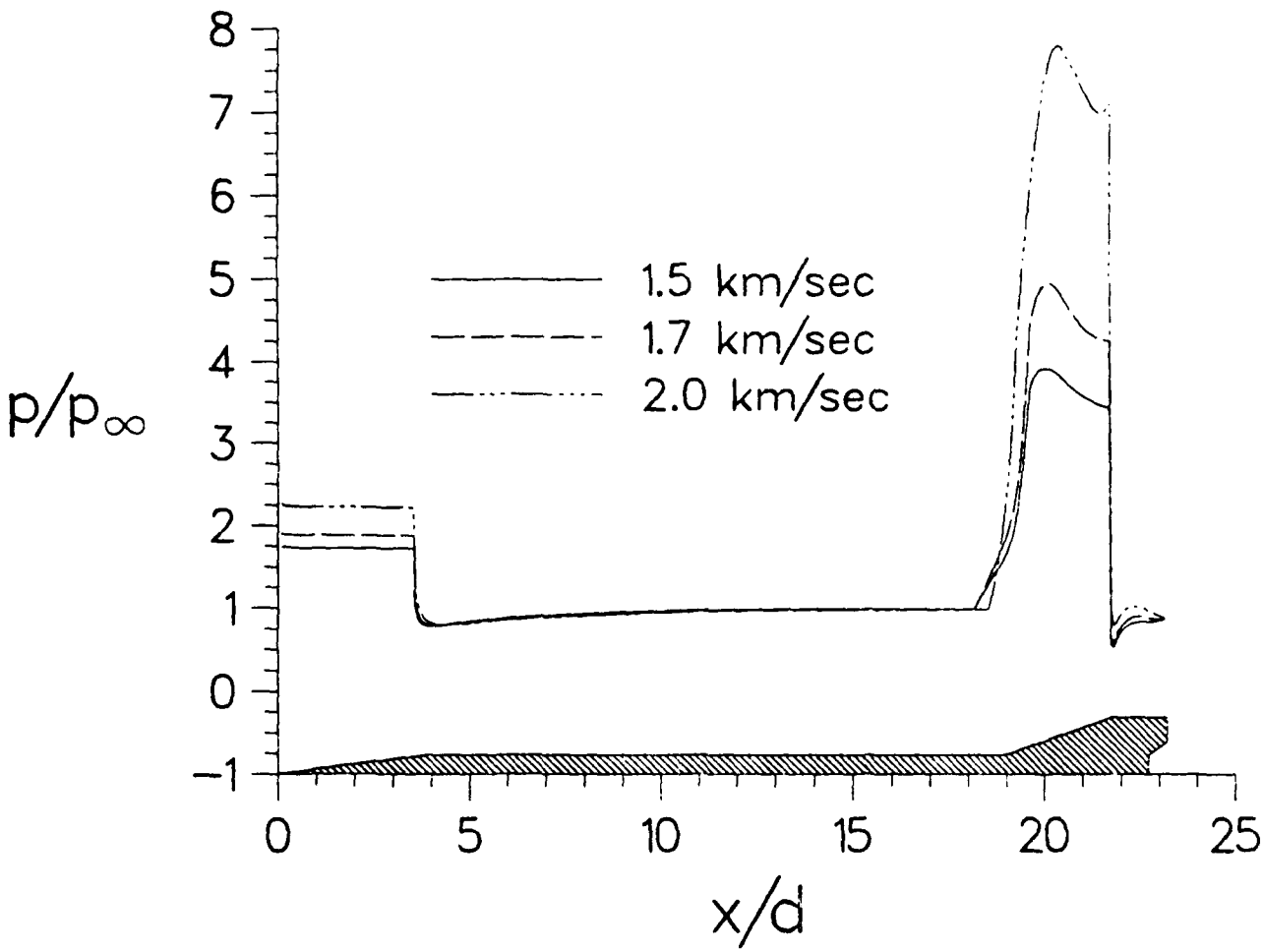

Figure 6. Computed Forebody and Fin Leading Edge Surface Pressure for M829, V_∞=1.5, 1.7, & 2.0 km/sec, $\alpha = 0°$

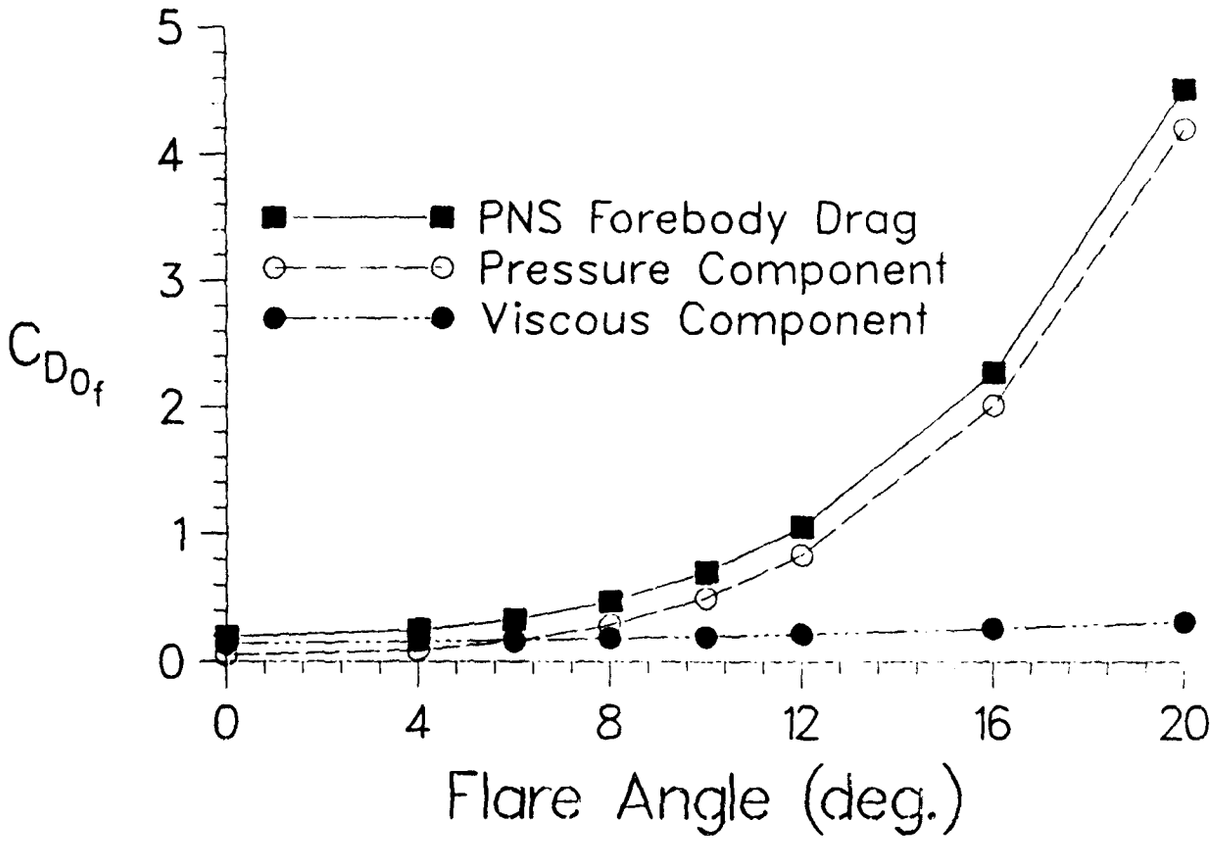

Figure 7. Computed Zero-Yaw Forebody Drag Components for F829 With Various Flare Angles, V_∞=1.5 km/sec, $\alpha = 0°$

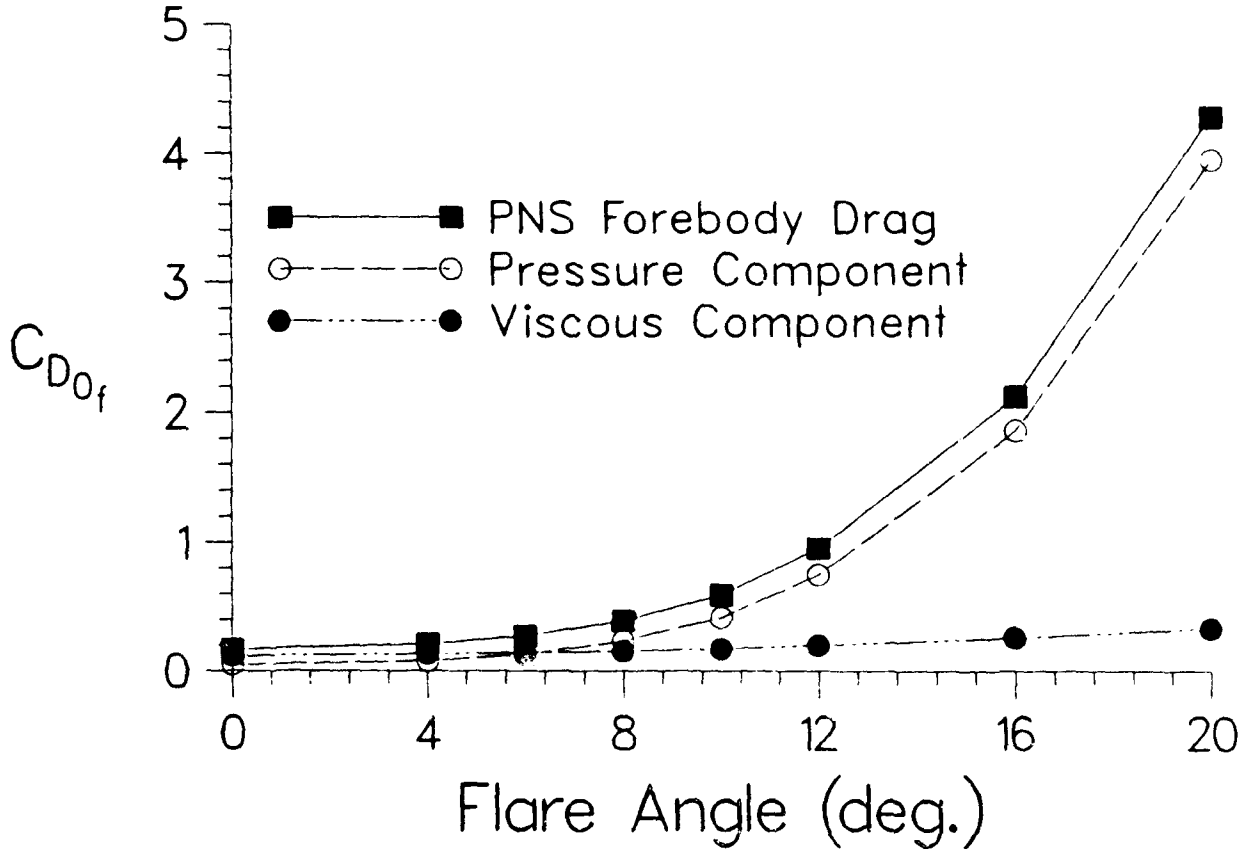

Figure 8. Computed Zero-Yaw Forebody Drag Components for F829 With Various Flare Angles, V_∞=2.0 km/sec, $\alpha = 0°$

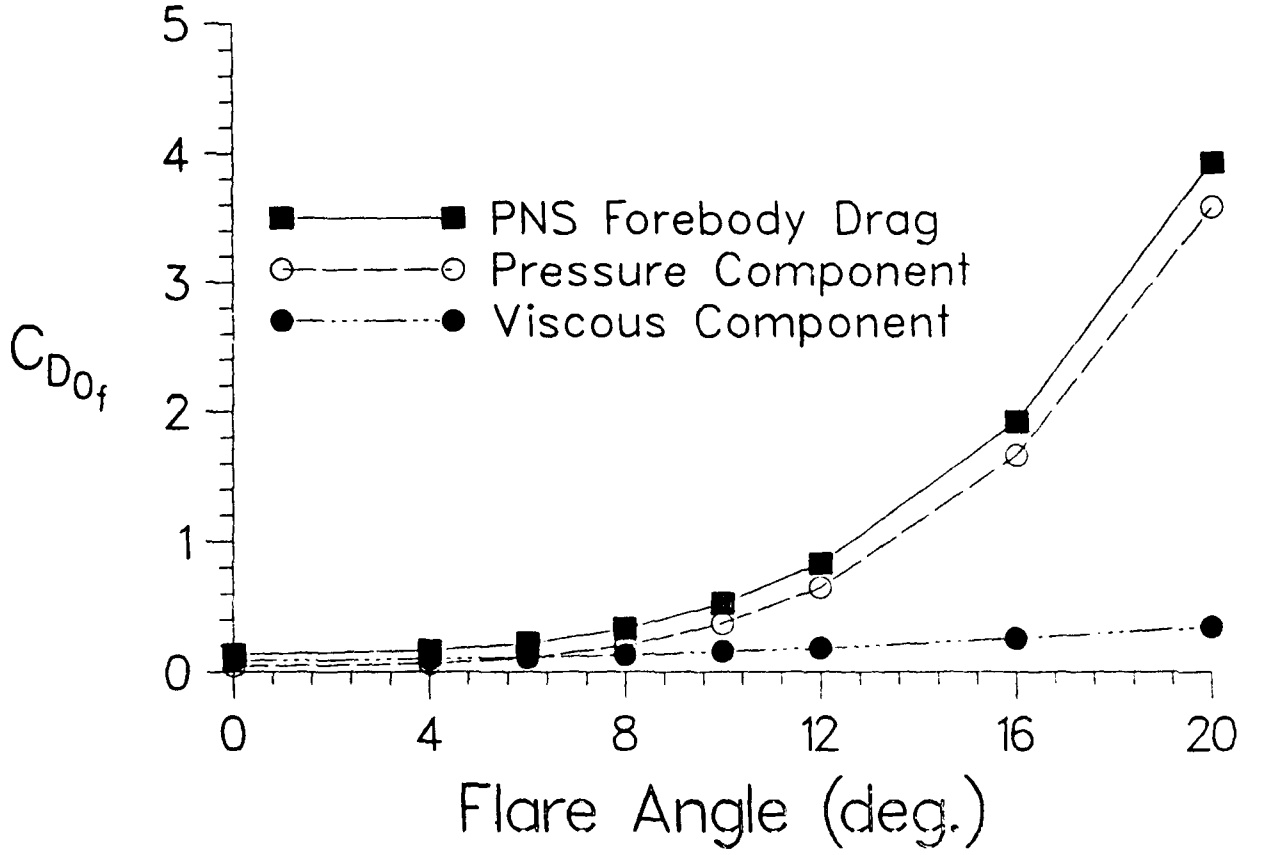

Figure 9. Computed Zero-Yaw Forebody Drag Components for F829 With Various Flare Angles, V_∞=3.0 km/sec, $\alpha = 0°$

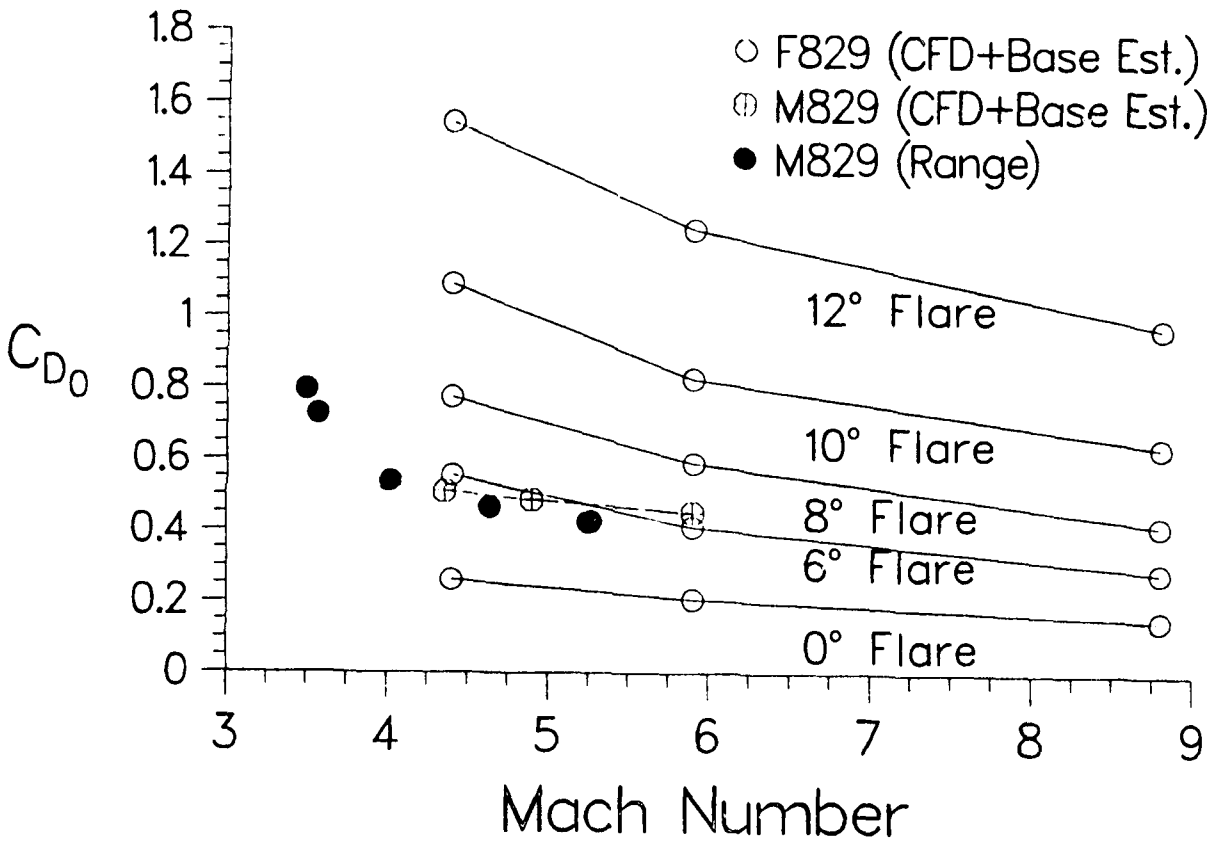

Figure 10. Comparison of Computed and Measured Zero-Yaw Drag Coefficients for F829 Configuration and M829 Projectile

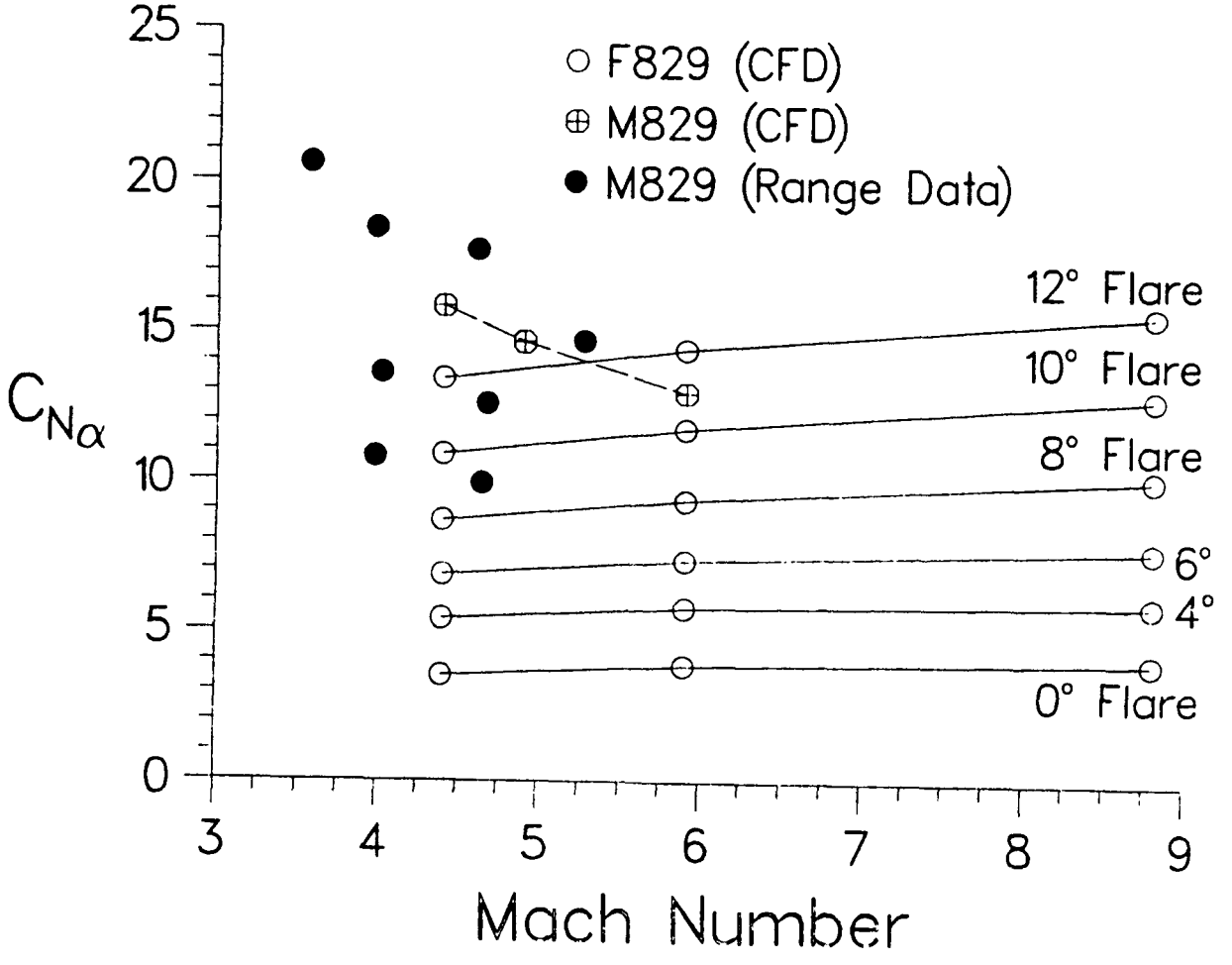

Figure 11. Comparison of Computed and Measured Normal Force Coefficient for F829 Configuration and M829 Projectile

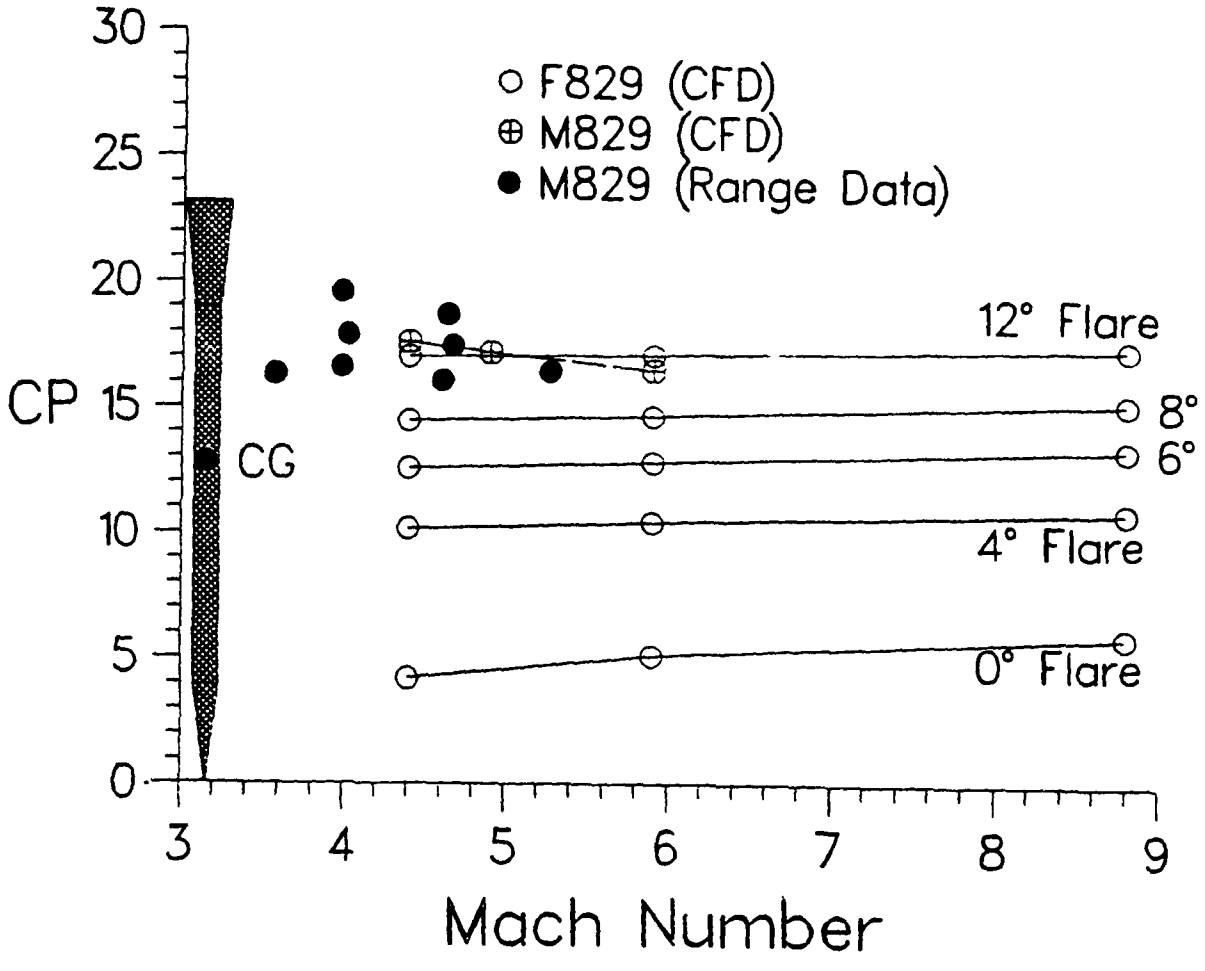

Figure 12. Comparison of Computed and Measured Normal Force Center of Pressure for F829 Configuration and M829 Projectile

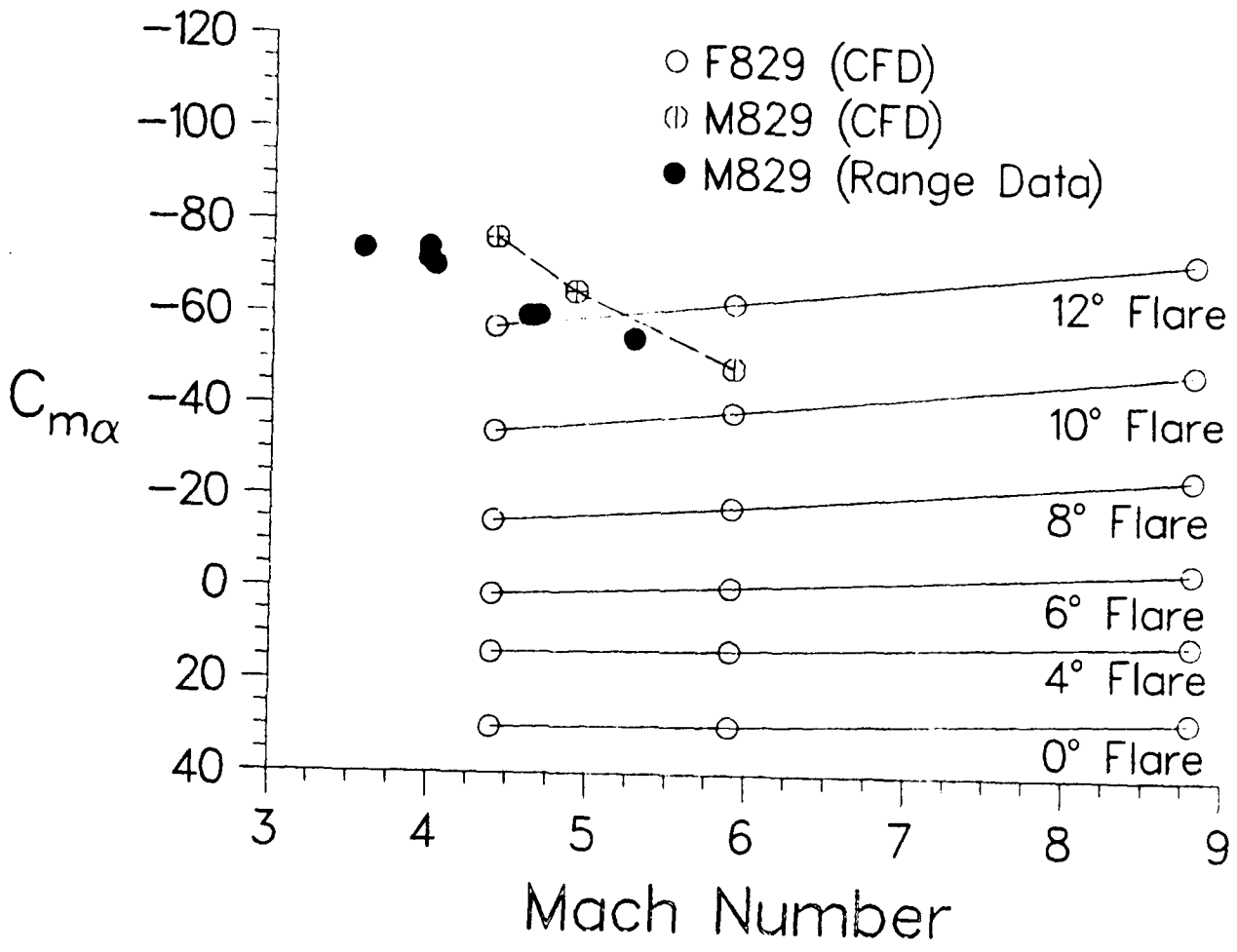

Figure 13. Comparison of Computed and Measured Pitching Moment Coefficient for F829 Configuration and M829 Projectile

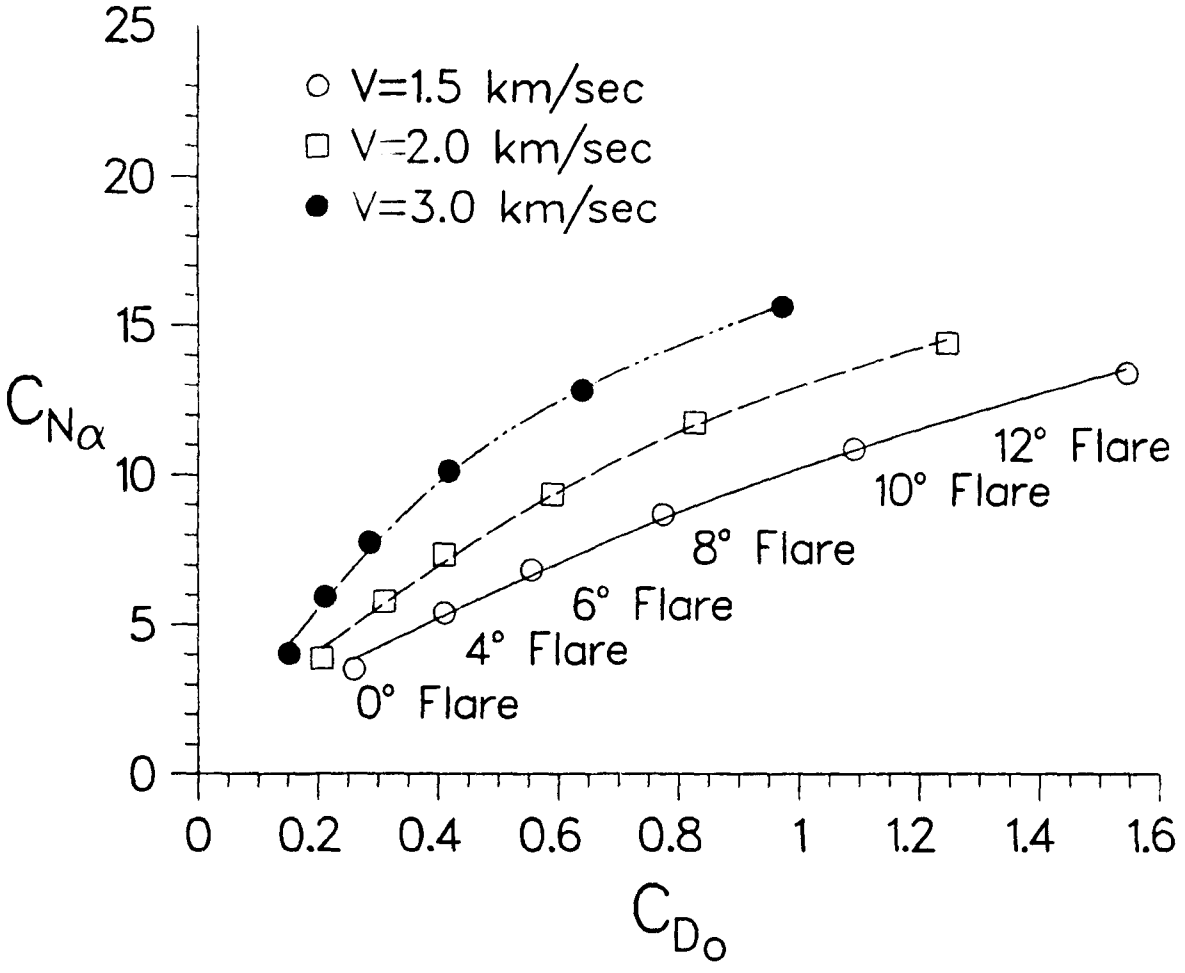

Figure 14. Computed Normal Force Coefficient Versus Zero-Yaw Drag Coefficient for F829 with Various Flare Angles

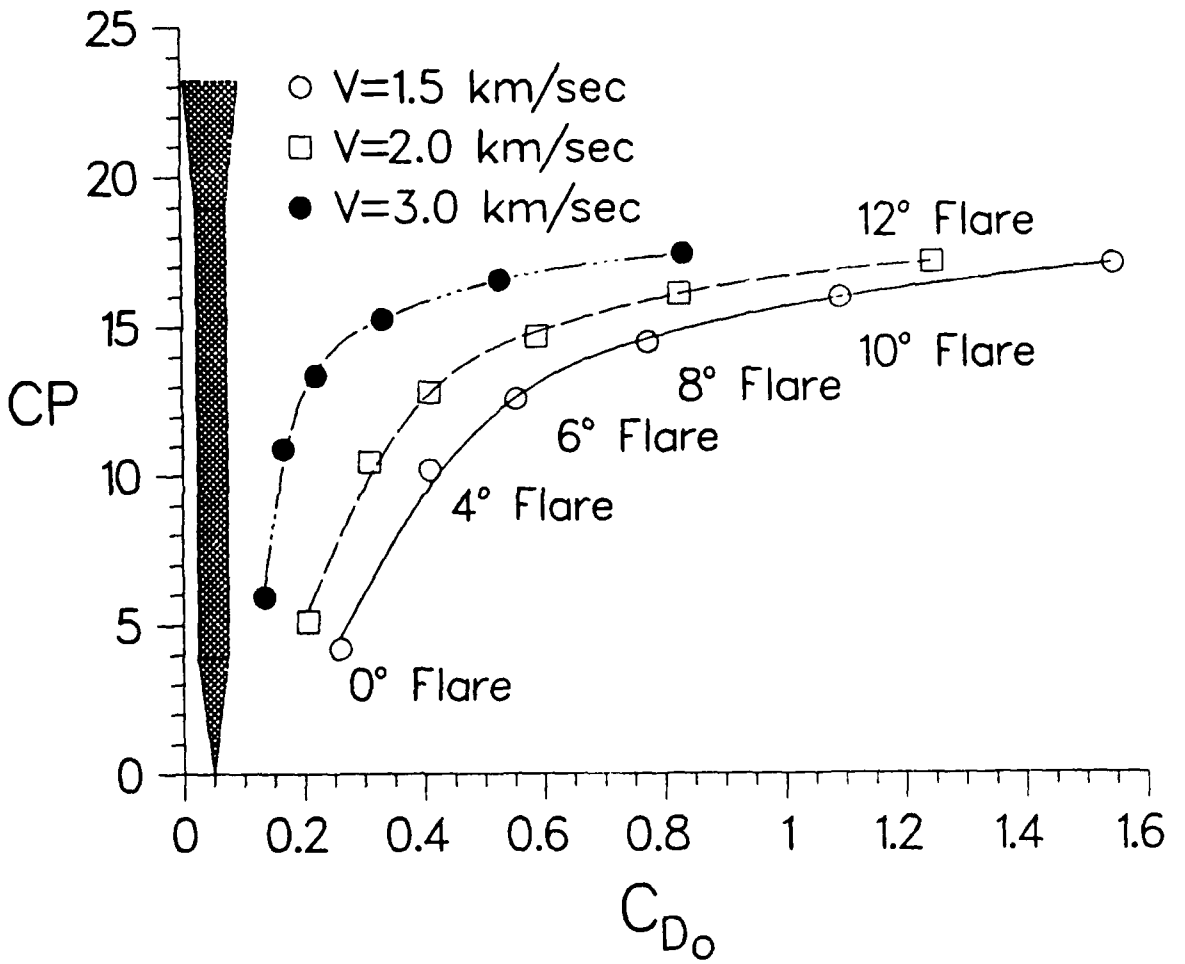

Figure 15. Computed Center of Pressure Versus Zero-Yaw Drag Coefficient for F829 with Various Flare Angles

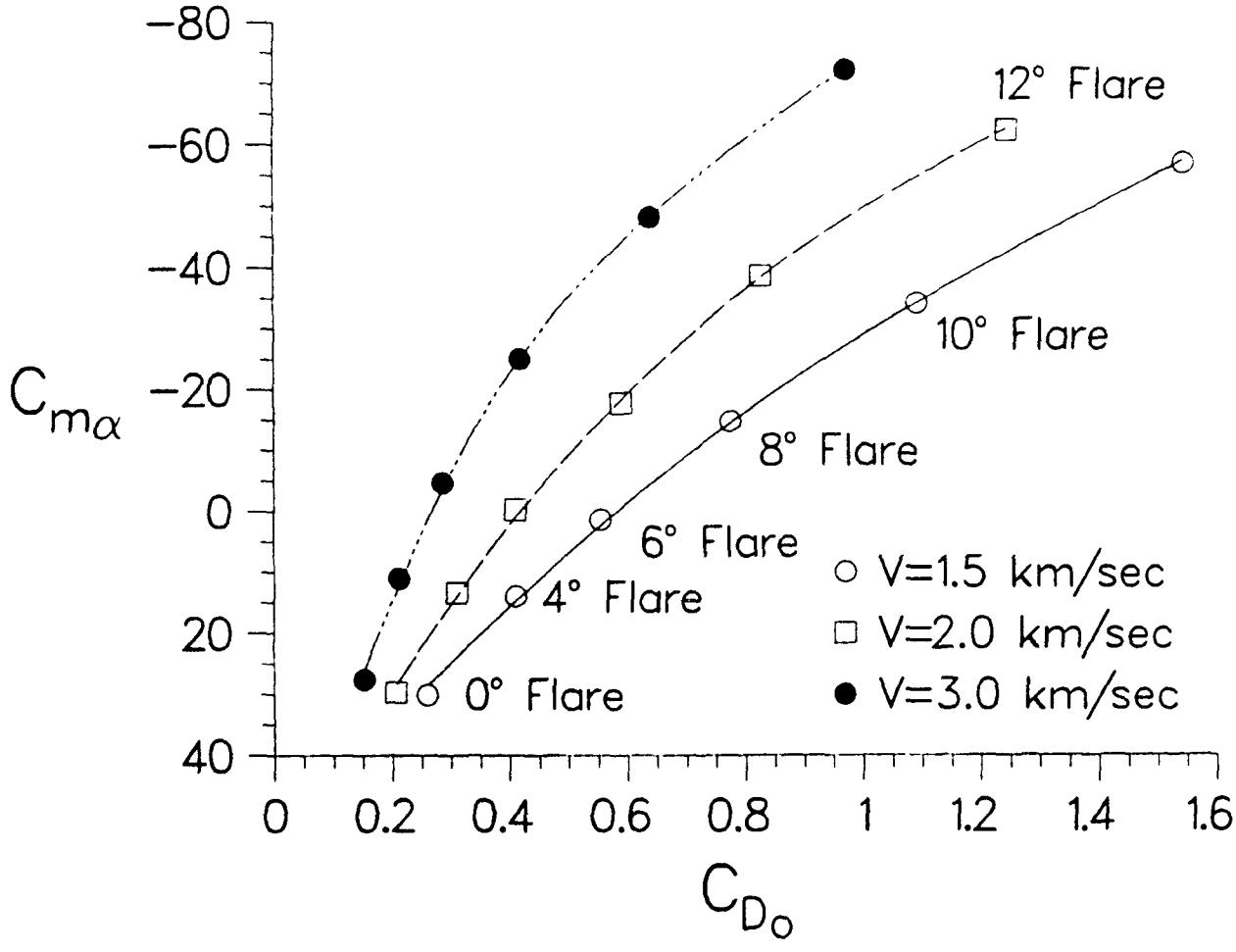

Figure 16. Computed Pitching Moment Coefficient Versus Zero-Yaw Drag Coefficient for F829 with Various Flare Angles

6. REFERENCES

Baldwin, B.S., and H. Lomax. "Thin-Layer Approximation and Algebraic Model for Separated Turbulent Flows," AIAA Paper No. 78-0257, January 1978.

Beam, R., and R.F. Warming. "An Implicit Factored Scheme for the Compressible Navier-Stokes Equations," AIAA Journal, Vol. 16, No. 4, pp. 393-402, 1978.

Guidos, B.J., and P. Weinacht. "Parabolized Navier-Stokes Computation of Surface Heat Transfer Characteristics for Supersonic and Hypersonic KE Projectiles," U.S. Army Research Laboratory, Aberdeen Proving Ground, Maryland, ARL-TR-191, August 1993.

Guidos, B.J.. "External Flow Computations for a Finned 60mm Ramjet in Steady Supersonic Flow," U.S. Army Ballistic Research Laboratory, Aberdeen Proving Ground, Maryland, BRL-MR-3801, December 1989. (AD A216998)

Guidos, B.J., P. Weinacht, and D.S. Dolling. "Comparison of Navier-Stokes Computation and Experiment for Pointed, Spherical, and Flat Tipped Shell at Mach 2.95 " U.S. Army Ballistic Research Laboratory, Aberdeen Proving Ground, Maryland, BRL-MR-3076, January 1990. (AD A218749)

Heyser, A., F. Maurer, and E. Oberdorffer."Experimental Investigation on the Effect of Tail Surfaces and Angle of Attack on Base Pressure in Supersonic Flow," NATO Advisory Group for Aerospace Research and Development (AGARD) Conference Proceedings No. 10, The Fluid Dynamic Aspects of Ballistics, pp. 267-290, September 1966.

McCoy, R.L.. " 'McDrag'- A Computer Program for Estimating the Drag Coefficients of Projectiles," U.S. Army Ballistic Research Laboratory, Aberdeen Proving Ground, Maryland, ARLBRL-TR-02293, February 1981. (AD A09810)

Murphy, C.H.. "Free Flight Motion of Symmetric Missiles," U.S. Army Ballistic Research Laboratories, Aberdeen Proving Ground, Maryland, BRL Report No. 1216, July 1963. (AD A442757)

Rai, M.M., and D.S. Chaussee. "New Implicit Boundary Procedures: Theory and Applications," AIAA Paper No. 83-0123, January 1983.

Schiff, L.B., and J.L. Steger. "Numerical Simulation of Steady Supersonic Flow," AIAA Paper No. 79-0130, January 1979.

Schiff, L.B., and W.B. Sturek. "Numerical Simulation of Steady Supersonic Flow over an Ogive Cylinder Boattail Body," U.S. Army Ballistic Research Laboratory, Aberdeen Proving Ground, Maryland, ARBRL-TR-02363, September 1981. (AD 106060)

Sedney, R.. "Review of Base Drag," NATO Advisory Group for Aerospace Research and Development (AGARD) Conference Proceedings No. 10, The Fluid Dynamic Aspects of Ballistics, pp. 215-240, September 1966.

Sturek, W.B., and L.B. Schiff. "Computations of the Magnus Effect for Slender Bodies in Supersonic Flow," U.S. Army Ballistic Research Laboratory, Aberdeen Proving Ground, Maryland, ARBRL-TR-02384, December 1981. (AD 110016)

Weinacht, P. "Application of Computational Fluid Dynamics to the Analysis of the Aerodynamics of a Railgun Projectile," U.S. Army Ballistic Research Laboratory, Aberdeen Proving Ground, Maryland, ARBRL-MR-3742, March 1989. (AD A207758)

Weinacht, P., B.J. Guidos, L.D. Kayser, and W.B. Sturek. "PNS Computations for Spinning and Fin-Stabilized Projectiles at Supersonic Speeds," U.S. Army Ballistic Research Laboratory, Aberdeen Proving Ground, Maryland, ARBRL-MR-3464, September 1985. (AD A160393)

Weinacht, P., B.J. Guidos, W.B. Sturek, and B.A. Hodes. "PNS Computations for Spinning Shell at Moderate Angles of Attack and for Long L/D Finned Projectiles," U.S. Army Ballistic Research Laboratory, Aberdeen Proving Ground, Maryland, BRL-MR-3522, June 1986. (AD 169531)

Weinacht, P., and W.B. Sturek. "Computation of the Roll Characteristics of Finned Projectiles," BRL-TR-2931, U.S. Army Ballistic Research Laboratory, Aberdeen Proving Ground, Maryland, June 1988. (AD 197875)

Weinacht, P., and W.B. Sturek. "Navier-Stokes Predictions of Pitch Damping for Finned Projectiles using Steady Coning Motion," AIAA Paper 90-3088, August 1990.

Weinacht, P., W. Sturek, and L. Schiff. "Navier-Stokes Predictions of Pitch Damping for Axisymmetric Shell using Steady Coning Motion," AIAA Paper 91-2855, August 1991.

LIST OF SYMBOLS

a	speed of sound
C_{D_0}	zero-yaw drag coefficient
$C_{D_{0_B}}$	zero-yaw base (and fin trailing edge) drag coefficient
$C_{D_{0_f}}$	zero-yaw forebody drag coefficient
C_{m_α}	pitching moment coefficient, evaluated as C_m/α, α in radians
C_{N_α}	normal force coefficient, evaluated as C_N/α, α in radians
CP	normal force center of pressure, calibers from pointed nosetip
d	reference diameter of projectile
$\hat{E}, \hat{F}, \hat{G}$	inviscid flux vectors of transformed gas dynamic equations
$\hat{H}_c$	inviscid source term for cylindrical coordinate formulation of transformed gas dynamic equations
l	reference length
p	pressure
$\bar{Q}$	vector of dependent variables of gas dynamic equations
$\hat{Re}$	freestream sonic Reynolds number, $\rho_\infty a_\infty d/\mu_\infty$
Re_m	freestream Reynolds number, $\rho_\infty V_\infty l/\mu_\infty$, based on a reference length of 1 meter
$\hat{S}$	viscosity vector of transformed gas dynamic equations
$\hat{S}_c$	viscous source term for cylindrical coordinate formulation of transformed gas dynamic equations
V	velocity
u, v, w	velocity components in x, y, z directions
x, y, z	physical Cartesian coordinates

Greek Symbols

α	total angle of attack; pitch angle; yaw angle
ϵ	total energy per unit volume of fluid
μ	coefficient of molecular viscosity
ρ	density
ξ, η, ζ	transformed coordinates

Subscript

∞	freestream condition
B	projectile base condition

INTENTIONALLY LEFT BLANK.

No. of Copies	Organization
2	Administrator Defense Technical Info Center ATTN: DTIC-DDA Cameron Station Alexandria, VA 22304-6145
1	Commander U.S. Army Materiel Command ATTN: AMCAM 5001 Eisenhower Ave. Alexandria, VA 22333-0001
1	Director U.S. Army Research Laboratory ATTN: AMSRL-OP-SD-TA, Records Management 2800 Powder Mill Rd. Adelphi, MD 20783-1145
3	Director U.S. Army Research Laboratory ATTN: AMSRL-OP-SD-TL, Technical Library 2800 Powder Mill Rd. Adelphi, MD 20783-1145
1	Director U.S. Army Research Laboratory ATTN: AMSRL-OP-SD-TP, Technical Publishing Branch 2800 Powder Mill Rd. Adelphi, MD 20783-1145
2	Commander U.S. Army Armament Research, Development, and Engineering Center ATTN: SMCAR-TDC Picatinny Arsenal, NJ 07806-5000
1	Director Benet Weapons Laboratory U.S. Army Armament Research, Development, and Engineering Center ATTN: SMCAR-CCB-TL Watervliet, NY 12189-4050
1	Director U.S. Army Advanced Systems Research and Analysis Office (ATCOM) ATTN: AMSAT-R-NR, M/S 219-1 Ames Research Center Moffett Field, CA 94035-1000

No. of Copies	Organization
1	Commander U.S. Army Missile Command ATTN: AMSMI-RD-CS-R (DOC) Redstone Arsenal, AL 35898-5010
1	Commander U.S. Army Tank-Automotive Command ATTN: AMSTA-JSK (Armor Eng. Br.) Warren, MI 48397-5000
1	Director U.S. Army TRADOC Analysis Command ATTN: ATRC-WSR White Sands Missile Range, NM 88002-5502
1	Commandant U.S. Army Infantry School ATTN: ATSH-WCB-O Fort Benning, GA 31905-5000
	Aberdeen Proving Ground
2	Dir, USAMSAA ATTN: AMXSY-D AMXSY-MP, H. Cohen
1	Cdr, USATECOM ATTN: AMSTE-TC
1	Dir, USAERDEC ATTN: SCBRD-RT
1	Cdr, USACBDCOM ATTN: AMSCB-CII
1	Dir, USARL ATTN: AMSRL-SL-I
5	Dir, USARL ATTN: AMSRL-OP-AP-L

No. of Copies	Organization
11	Commander US Army Armament RD&E Center ATTN: SMCAR-AET-A, S. Kahn C. Ng M. Amoruso H. Hudgins J. Grau E. Brown B. Wong W. Toledo S. Chung C. Livecchia G. Malejko Picatinny Arsenal, NJ 07806-5000
3	Commander US Army Armament RD&E Center ATTN: SMCAR-CCH-V, B. Konrad E. Fennell T. Louzeiro Picatinny Arsenal, NJ 07806-5000
4	Commander US Army Armament RD&E Center ATTN: SMCAR-FSE, A. Graf D. Ladd E. Andricopoulis K. Cheung Picatinny Arsenal, NJ 07806-5000
1	Commander US Army Missile Command ATTN: AMSMI-RD-SS-AT, B. Walker Redstone Arsenal, AL 35898-5010
3	U.S. Army Research Office ATTN: G. Anderson K. Clark T. Doligowski P.O. Box 12211 Research Triangle Park, NC 27709-2211

No. of Copies	Organization
2	Director US Army ERDEC ATTN: SCBRD-RTB, D. Weber F. Wrede Aberdeen Proving Ground, MD 21010-5423
2	Director US Army Research Laboratory ATTN: AMSRL-MA-CA, M.R. Fletcher M.E. O'Day 405 Arsenal St. Watertown, MA 02172-0001
2	United States Military Academy Department of Civil and Mechanical Engineering ATTN: M. Costello A. Dull West Point, NY 10996
6	Director National Aeronautics and Space Administration Ames Research Center ATTN: MS-258-1, L. Schiff T. Holst D. Chaussee T. Edwards G. Molvik S. Lawrence Moffett Field, CA 94035
3	Director National Aeronautics and Space Administration Langley Research Center ATTN: Technical Library J. South M. Rai Langley Station Hampton, VA 23665

No. of Copies	Organization
3	Air Force Armament Laboratory ATTN: AFATL/FXA, B. Simpson G. Abate R. Adelgren Eglin AFB, FL 32542-5434
2	Commander US Naval Surface Warfare Center Applied Mathematics Branch ATTN: Code R44, A. Wardlaw Code R44, F. Priolo White Oak Laboratory Silver Spring, MD 20903-5000
1	Commander US Naval Surface Weapons Center ATTN: F. Moore Dahlgren, VA 22448
2	USAF Wright Aeronautical Laboratories ATTN: AFWAL/FIMG, J. Shang WPAFB, OH 45433-6553
1	Arnold Engineering & Development Center Calspan Field Service ATTN: MS 600, J. Benek AAFS, TN 37389
2	Director Sandia National Laboratories ATTN: W. Oberkampf W. Wolfe Division 1636 Albuquerque, NM 87185
1	Los Alamos National Laboratory ATTN: MS G770, W. Hogan Los Alamos, NM 87545

No. of Copies	Organization
3	Institute for Advanced Technology University of Texas at Austin ATTN: W. Reinecke T. Kiehne D. Barnett 4030-2 W. Braker Lane Austin, TX 78759-5329
2	University of California, Davis Department of Mechanical Engineering ATTN: H. Dwyer B. Meakin Davis, CA 95616
1	University of Maryland Department of Aerospace Engr. ATTN: J. Anderson Jr. College Park, MD 20742
1	University of Texas Department of Aerospace Engineering and Engineering Mechanics ATTN: D. Dolling Austin, Texas 78712-1055
2	University of Delaware Department of Mechanical Engineering ATTN: J. Danberg L. Schwartz Newark, DE 19716
1	University of Cincinnati Department of Aerospace Engineering ATTN: S. Rubin Mail Location 70 Cincinnati, OH 45221
1	University of Florida Department of Engineering Sciences College of Engineering ATTN: C. Hsu Gainesville, FL 32611

No. of Copies	Organization
1	MDA Engineering, Inc. ATTN: J. Steinbrenner 500 E. Border St., Suite 401 Arlington, TX 76010
2	Alliant Techsystems, Inc. ATTN: M. Swenson R. Burretta Mail Station MN48-3700 7225 Northland Dr. Brooklyn Park, MN 55428
1	General Research Corp. ATTN: H. King P.O. Box 6770 Santa Barbara, CA 93160-6770
5	Kaman Sciences Corp. ATTN: J. Forkois T. Hayden W. Leonard R. Prozan E. Statton 1500 Garden of the Gods Rd. Colorado Springs, CO 80907

USER EVALUATION SHEET/CHANGE OF ADDRESS

This Laboratory undertakes a continuing effort to improve the quality of the reports it publishes. Your comments/answers to the items/questions below will aid us in our efforts.

1. ARL Report Number ARL-MR-184 Date of Report September 1994

2. Date Report Received _____

3. Does this report satisfy a need? (Comment on purpose, related project, or other area of interest for which the report will be used.) _____

4. Specifically, how is the report being used? (Information source, design data, procedure, source of ideas, etc.) _____

5. Has the information in this report led to any quantitative savings as far as man-hours or dollars saved, operating costs avoided, or efficiencies achieved, etc? If so, please elaborate. _____

6. General Comments. What do you think should be changed to improve future reports? (Indicate changes to organization, technical content, format, etc.) _____

CURRENT ADDRESS

_____
Organization

_____
Name

_____
Street or P.O. Box No.

_____
City, State, Zip Code

7. If indicating a Change of Address or Address Correction, please provide the Current or Correct address above and the Old or Incorrect address below.

OLD ADDRESS

_____
Organization

_____
Name

_____
Street or P.O. Box No.

_____
City, State, Zip Code

(Remove this sheet, fold as indicated, tape closed, and mail.)
(DO NOT STAPLE)

DEPARTMENT OF THE ARMY

OFFICIAL BUSINESS

NO POSTAGE
NECESSARY
IF MAILED
IN THE
UNITED STATES

BUSINESS REPLY MAIL
FIRST CLASS PERMIT NO 0001, APG, MD

Postage will be paid by addressee

Director
U.S. Army Research Laboratory
ATTN: AMSRL-OP-AP-L
Aberdeen Proving Ground, MD 21005-5066